Journal of
Synchrotron
Radiation

ISSN 0909-0495

Received 3 April 2006
Accepted 1 August 2006

Strategies for data collection and calibration with a pinhole-geometry SAXS instrument on a synchrotron beamline

David Cookson,[a,b]* Nigel Kirby,[c] Robert Knott,[d] Myungae Lee[a] and David Schultz[a]

[a]ChemMatCARS, Advanced Photon Source, Argonne National Laboratory, Argonne, IL, USA, [b]Australian Synchrotron Research Program, Australian Nuclear Science and Technology Organisation, Building 434, Argonne, IL 60439, USA, [c]Australian Synchrotron, Clayton, Victoria, Australia, and [d]ANSTO, Private Mail Bag, Menai, NSW 2234, Australia. E-mail: cookson@cars.uchicago.edu

Undulator X-ray sources on third-generation synchrotrons have pushed small-angle X-ray scattering (SAXS) to the forefront of techniques in nanoscience and technology. With higher X-ray fluxes and improved focusing, it is usually the scattered intensity detector that places the most serious limitations on the overall capabilities of the instrument. Incorporating relatively simple components like point detectors, scattering standards, masking filters and in-line sample visualization into the flight tube of a pinhole-geometry SAXS camera can do much to mitigate these limitations. How these enhancements can be incorporated into routine data collection is demonstrated on the ChemMatCARS SAXS instrument, which utilizes pinhole geometry with an undulator insertion device at sector 15 of the Advanced Photon Source. In addition, with an X-ray energy range of 6–32 keV (2.0–0.4 Å) and an energy resolution of 10^{-4} $\Delta E/E$, this instrument can measure anomalous SAXS over a wide variety of atom species, with reliable normalization of scattered data.

Keywords: small-angle X-ray scattering; wide-angle X-ray scattering.

1. Introduction

The SAXS/WAXS instrument at ChemMatCARS, sector 15 of the Advanced Photon Source (Chicago, USA), is in many ways typical of modern undulator-based SAXS cameras and serves as a good example of the issues that arise when a traditional pinhole scattering geometry is coupled with a brilliant undulator source. The instrument is dedicated primarily to static and dynamic condensed matter chemistry and materials science, and is one of three general techniques (SAXS/WAXS, reflectivity and crystallography) used to meet the objectives of the ChemMatCARS sector. The basic parameters of the SAXS/WAXS camera (Table 1) result from high-quality beam delivery optics, but it is the additional hardware incorporated into the overall control system that allows even relatively inexperienced users to collect high-quality reproducible data from a wide range of nanostructured systems.

2. Instrument collimation

The ChemMatCARS SAXS/WAXS camera utilizes the radiation from a type-A undulator on the high-brilliance ring at the Advanced Photon Source (APS). Fig. 1 shows the basic collimation design of the instrument which utilizes a double-crystal monochromator (DCM) with water-cooled diamonds in a (111) orientation (Graber *et al.*, 1998). A pair of mirrors provides harmonic rejection and a 1:1 focus in the vertical direction with the option of bare silicon, rhodium or platinum stripes. Three pairs of crossed slits and one guard aperture provide the required collimation which, in conjunction with a 6.8 m flight tube, allow a minimum scattering angle (2θ) of 0.02° giving a minimum momentum transfer ($q = 4\pi\sin\theta/\lambda$) of 0.0015 Å^{-1} when using λ = 1.5 Å wavelength X-rays. To minimize parasitic scattering in the SAXS mode, about a quarter of the available beam in the horizontal and all the

Table 1
Specifications of the SAXS/WAXS camera on the ChemMatCARS beamline.

X-ray energy range	6–32 keV
X-ray wavelength range	2.0–0.4 Å
Energy resolution (diamond 111 DCM)	10^{-4} $\Delta E/E$
Energy reproducibility at 10 keV	±0.1 eV
Vertical focusing (bent mirror)	1:1
Available camera lengths	0.6, 1.9, 6.8 m
Current beam-stop radius	2 mm
Maximum camera exit-window radius	127 mm
q_{min} (1.5 Å, 6.8 m SAXS mode)	0.0015 Å^{-1}
q_{max} (0.42 Å, WAXS mode)	8.0 Å^{-1}
Maximum beam size (restricted to minimize parasitic scatter at 8.3 keV)	500 µm × 200 µm (H × V)
Estimated intensity (0.5 mm × 0.2 mm beam)	2×10^{12} photons s^{-1}

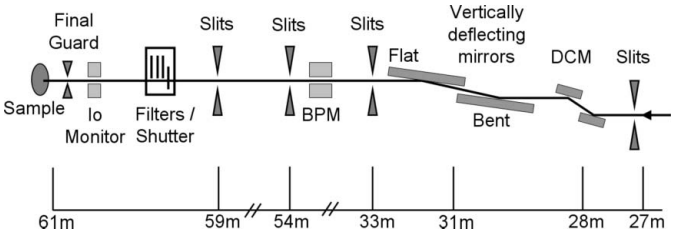

Figure 1
ChemMatCARS (15-ID) SAXS/WAXS camera collimation.

focused beam in the vertical is accepted, giving a typical beam size of 0.5 mm × 0.2 mm (horizontal × vertical). This gives an approximate intensity of 2×10^{12} photons s^{-1} with an energy resolution ($\Delta E/E$) from the DCM of $\sim 10^{-4}$.

Again to minimize the parasitic scattering, the monochromatic beam has to be stable to a few tens of micrometres at the final guard aperture. This is achieved *via* active feedback from a beam-position monitor (BPM) to a piezo-actuator on the θ rotation of the second diamond crystal in the DCM. The BPM uses the fluorescence from a chromium foil in the beam path to provide a difference over sum signal from an array of four photodiodes. The photon intensity just prior to the sample (I_0) is monitored with another PIN photodiode array that intersects the Laue scattering from a 10 µm mica foil. Unlike an ion chamber or a fluorescing metal foil, this adds negligible small-angle scatter to the beam, an important consideration close to the sample position. For the sample-in-air configuration, the vacuum-to-air window just before the sample is a 0.2 µm-thick silicon nitride membrane, while the air-to-vacuum window in the detector flight-tube is usually a mica foil, less than 50 µm thick.

The entire camera can be moved on precision rails and jacks to accommodate a large array of sample environments, including windowless in-vacuum operation and heavy-duty sample processing such as fibre spinning (Ran *et al.*, 2004). The entire system including collimation optics, sample manipulation and data acquisition is controlled by one GUI-based software package, *Saxs15id*, which provides users with a high degree of automation and presents normalized one-dimensional SAXS profiles to the user in real time (Cookson, 2006).

For weakly scattering samples at the lowest q range, it is essential to optimize the beam collimation to minimize parasitic scatter around the beam stop. This is initially facilitated by using the in-line specimen visualization system and the visible-light fluorescence from a thin phosphor screen in the specimen position. Final optimization of signal to noise is achieved with fine automated scans of critical slits correlated with full X-ray CCD images.

3. Data-collection strategy I: optimizing accessible q range

With flight-tube lengths ranging from 0.6 to 6.8 m, a wide span of q can be covered with significant regions of overlap. At even the longest camera length using a photon wavelength of 1.5 Å, a detector with 10 cm × 10 cm active area can subtend sufficient angular range to span more than one order of magnitude in q range. As form-factor scattering tends to decay as the fourth power of the scattering angle, it is often the dynamic range of a CCD detector rather than its physical size that limits the measurable q range. The best way to access different q ranges is to change camera length and a primary design goal of this facility was to allow the camera flight-tube length to be altered as quickly as possible.

Fig. 2 shows the CCD detector located outside the flight tube, with mechanical infrastructure that allows the camera length to be changed and returned to operation in as little as 15 min with minimal manual labour. A high-capacity PLC-controlled pumping system allows an automatic venting or evacuation cycle of even the longest camera length in less than 3 min.

In order to take full advantage of the mechanical features of this system, a number of components have been built into the camera design to assist with the small but important adjustments that must be made to re-align the camera after major changes in length. Fig. 3 indicates schematically the components that can be actuated automatically in computer-controlled sequences.

In the front module of the detector flight-tube a mechanism allows the insertion and retraction of an optical alignment mirror. This mirror, coupled with a high-magnification video camera, allows small samples or small sample regions (<50 µm) to be targeted reliably, free of parallax error. Using the video system in conjunction with PIN photodiodes

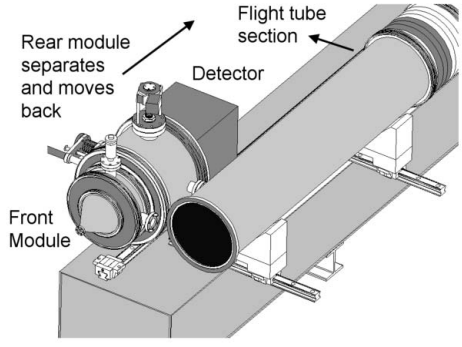

Figure 2
15-ID SAXS camera shown with minimum length. The rear module can be separated from the front module by a number of flight-tube segments.

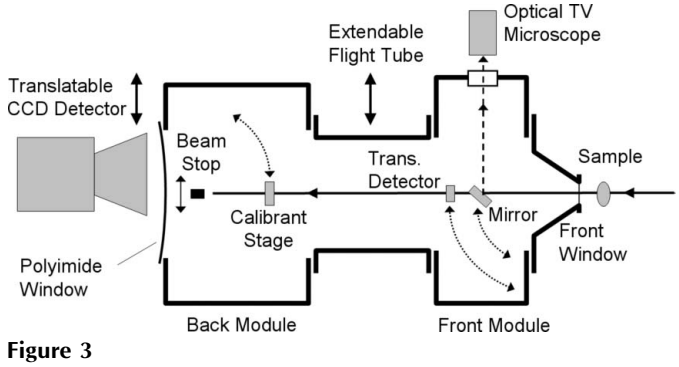

Figure 3
Camera flight-tube showing components than can be actuated under computer control.

embedded in both the beam stop and the calibration stage greatly reduces the time required to align the system and ensures that the CCD detector is not damaged by the direct X-ray beam.

The calibration stage in the rear module contains a mesoporous silica standard (Sheppard *et al.*, 2005) which, when placed in the beam, provides strong isotropic diffraction rings which are then used by the software to find the current beam centre with high accuracy. When studying isotropic scattering specimens the detector face can be moved relative to the centre of the scattering pattern, effectively increasing the q range with no loss of information. With an automated calibration sequence, the detector can be moved to the user requirements with minimal time lost to re-determining the beam centre.

4. Data-collection strategy II: compensating for dynamic range limitations

With a reliable measurement of I_0 provided by the mica-foil scattering detector just before the sample, all that is now needed is a good measurement of transmitted beam intensity, I_t, after the sample. While the photodiode in the beam stop can, in principle, provide this value, the small active area of the device makes it susceptible to minute fluctuations in the beam position. The transmission detector (Fig. 3) subtends a much larger scattering angle and is less prone to this source of variability. It is therefore the detector of choice when the camera is in sample transmission mode.

Even when rigorously normalizing blank and sample SAXS exposures to constant incident intensity and transmission, the resulting profiles may have features that are artifacts of the limited dynamic range of the detector. Fig. 4 demonstrates how the 'noise floor' and the saturation level of a typical CCD detector conspire to limit its effective dynamic range. The detector used for all measurements was a Bruker SMART 6000, with a phosphor optically coupled to a large-format CCD chip with a 1:1.2 fibre taper.

Ideally, scattering profiles measured with increasing exposure times plotted on a log intensity scale should translate upward with no change in gradient or shape. In practice, it is only for the longer exposure times that the curve at high q starts to separate from the inherent readout noise of the detector. Unlike thermal or 'dark current' noise, readout noise cannot be measured for a fixed time and then subtracted from the signal. Further, as readout noise is independent of incident X-ray intensity, Poisson statistics do not apply and averaging many short exposures is not particularly helpful. Only longer measurement times reliably mitigate this problem. Unfortunately, longer exposure times as shown in Fig. 4 tend to saturate the detector in the low-q region. Small regions of saturation can be ignored, but most CCD chips can only tolerate a certain number of saturated pixels before all the measured pixel intensities become unreliable. Multiple exposures taken with increasing acquisition times ensure that the limited dynamic range of a detector can be checked at every part of the measured q range. This is especially important when measuring a range of samples which may show markedly different scattering patterns.

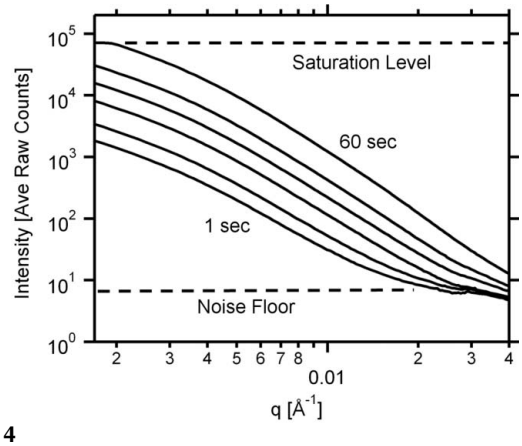

Figure 4
Profiles integrated from SAXS images of suspended alumina nanoparticles.

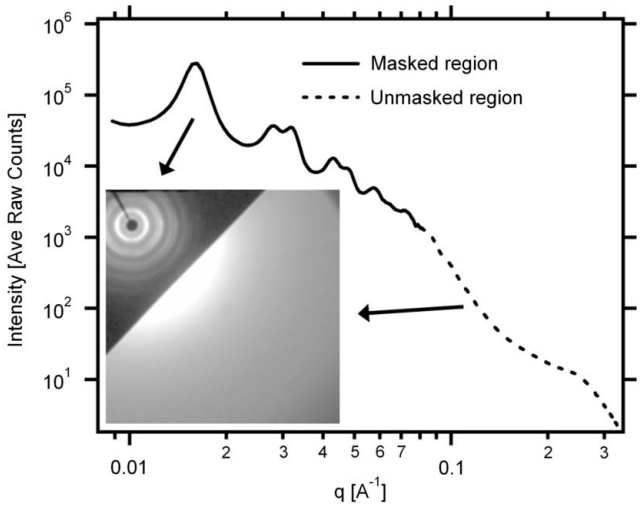

Figure 5
Selective masking of a SAXS exposure used to generate a spliced profile with enhanced dynamic range. The sample was an alumina membrane with cylindrical pores close-packed at a radius of 500 Å.

For specimens with a very large scattering intensity range, the software package *Saxs15id* will allow different integration regions on successive images to be spliced together, creating a total integrated profile with a very large effective dynamic range. These masking and partial region integration commands can also generate enhanced dynamic range profiles from single images where a semi-transparent mask has been used to reduce the scattered intensity close to the beam stop (Fig. 5).

5. Data-collection strategy III: ensuring adequate normalization

The detector scheme outlined previously usually ensures that the quality of normalization between different exposures is sufficient for most SAXS analyses. There are, however, situations when the linearity between the I_0 and I_t detectors

can change. This is most likely to happen when changing photon energy, as the underlying signal-generating mechanisms are different in the different detectors. In the case of I_0, the spots from the diffracting mica foil will move with changing incident energy, while the penetration depth of the direct beam into the active layer of the transmission photodiode will non-commensurately change its sensitivity. As a result, measurements such as transmission which rely on a constant relationship between the two detector sensitivities may have significant error.

The mesoporous silica sample in the back calibration stage scatters incident radiation into perfectly uniform rings, free of graininess or preferred orientation, making it relatively insensitive to small variations of stage placement. The integrated ring intensity therefore serves as an excellent secondary intensity calibration which will remain correlated to the transmitted beam intensity. Fig. 6 shows how scattering from the mesoporous silica irradiated by the transmitted beam can be used to normalize a series of exposures taken at different photon energies, effectively removing features due to the undulator intensity spectrum and specimen absorption.

The conversion from normalized profiles to absolute intensity is achieved with the use of secondary standards, primarily pure water (Orthaber *et al.*, 2000) and glassy carbon (Russell *et al.*, 1988). A recent publication (Dreiss *et al.*, 2006) has shown some of the relative merits of various intensity calibration standards. For weak scattering standards like pure water, some care must be taken to ensure adequate dynamic range over the q-range of interest. This is routinely done using multiple exposures taken with different exposure times as described in the previous section.

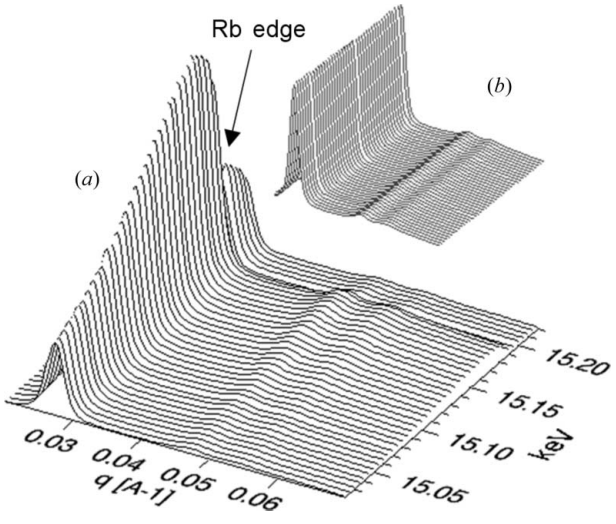

Figure 6
(*a*) Scattering profiles from a mesoporous silica standard built into the rear module of the SAXS camera at energies near the Rb *K*-edge. The primary scattering sample is a 0.5 *M* solution of RbCl situated in front of the flight tube. Using the integrated area of the silica peak above the background yields a normalization curve that can be used to normalize scattering over a range of energies (*b*).

6. Data-collection strategy IV: dealing with inhomogeneous or time-evolving samples

Primary reasons for the use of SAXS/WAXS techniques on a synchrotron radiation source include weak scatterers, high spatial resolution, fast kinetics and energy selection. Clearly the sample environment also plays a vital role in the acquisition of SAXS/WAXS data and special attention must be given to the fact that the sample scattering response may not be uniform over its entire volume. Such environments may be simple stretching apparatus (Finnigan *et al.*, 2005), or more complex shear environments such as the Linkam flat-plate shear cell (Sutton *et al.*, 2004), or even a complete fibre-spinning apparatus (Ran *et al.*, 2004). Pinpointing a specific region of interest on a particular sample is greatly facilitated by the in-line camera system previously discussed, but integrating the scattering measurements with automated scanning of environmental variables and sample position can bring additional insight to the hierarchy of structure present in synthetic and natural materials.

As an example, Fig. 7 shows a sample of PET polymer that has been folded along two axes. The resultant stresses along the folds in the material have given rise to induced nano-

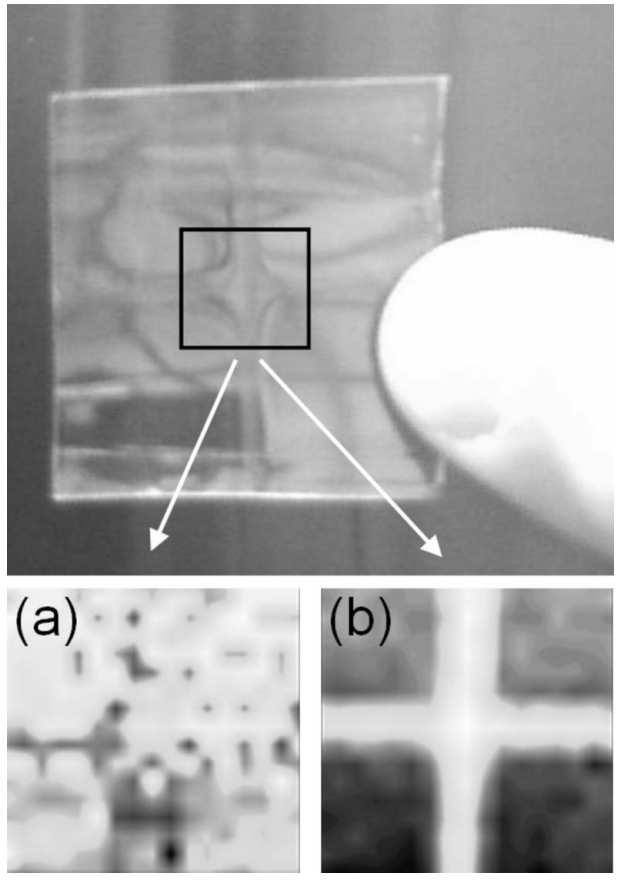

Figure 7
A creased piece of PET polymer formed nanocrystals along the fold lines. A radiograph (*a*) performed over the sub-region shown shows little contrast while the enhanced scattering into the q range of 0.03–0.04 Å^{-1} automatically generated from a series of SAXS measurements shows clear contrast of the fold lines (*b*).

crystallization. A regular radiograph (mapping X-ray transmission against a sample position on an x–y raster) shows almost no contrast. By studying the enhanced scattering at a q range of 0.03–0.04 Å^{-1}, however, a clear map of induced nano-crystallization emerges.

The software (*Saxs15id*) that integrates sample mesh scanning with SAXS measurement and subsequent processing can also control environmental parameters like temperature, stress, strain, tension, flow rate and photon energy.

The duty cycle time of repeated measurements is clearly an experimental constraint, especially for time-evolving systems. When using a Bruker CCD detector this is dominated by a readout time of 9 s (at full pixel resolution) which must be added to the actual exposure time. The other major component of the duty cycle arises from the insertion/retraction of the transmission detector ($\sim$9 s + counting time). In practice, unless there is substantial precipitation from a liquid sample or a change of irradiation energy, repeated transmission measurements are not required for the same sample. Sample movement time is generally negligible during scans, so the longest automated duty cycle usually applies to ASAXS scans. In this case each energy increment requires a transmission measurement and several exposures of different duration, giving typical duty cycle times of 30–60 s.

7. Conclusion

While much of the capabilities of undulator-based SAXS/WAXS facilities arise directly from the brilliant X-ray source, their greatest weaknesses lie in the limitations of most commercially available detector systems. Many of these limitations can be greatly mitigated with judicious use of relatively inexpensive enhancements to the scattering flight-tube infrastructure and the use of relatively simple protocols incorporated into the software and used routinely.

The extensive design/drafting work of F. Westferro and expert technical assistance of H. Brewer, G. Macha, J. VonOsinski, M. Bolbat and S. Ruan are gratefully acknowledged. ChemMatCARS sector 15 is principally supported by the National Science Foundation/Department of Energy under grant number CHE0087817 and by the Illinois Board of Higher Education. The Advanced Photon Source is supported by the US Department of Energy, Basic Energy Sciences, Office of Science, under Contract No. W-31-109-Eng-38.

References

Cookson, D. J. (2006). *Saxs15id – a software package for SAXS/WAXS data processing and analysis*, http://cars.uchicago.edu/chemmat.

Dreiss, C. A., Jack, K. S. & Parker, A. P. (2006). *J. Appl. Cryst.* **39**, 32–38.

Finnigan, B., Jack, K., Campbell, K., Halley, P., Truss, R., Casey, P., Cookson, D., King, S. & Martin, D. (2005). *Macromolecules*, **38**, 7386–7396.

Graber, T., Mini, S. M. & Viccaro, P. J. (1998). *Proc. SPIE*, **3448**, 256–265.

Orthaber, D., Bergmann, A. & Glatter, O. (2000). *J. Appl. Cryst.* **33**, 218–225.

Ran, S., Burger, C., Sics, I., Yoon, K., Fang, D., Kim, K. S., Avila-Orta, C., Keum, J., Chu, B., Hsiao, B. S., Cookson, D., Shultz, D., Lee, M., Viccaro, J. & Ohta, Y. (2004). *Colloid Polym. Sci.* **282**, 802–809.

Russell, T. P., Lin, J. S., Spooner, S. & Wignall, G. D. (1988). *J. Appl. Cryst.* **21**, 629–638.

Sheppard, D. A., Maitland, C. F. & Buckley, C. E. (2005). *J. Alloys Compd.* **404**, 405–408.

Sutton, D., Hanley, T., Knott, R. & Cookson, D. (2004). *J. Synchrotron Rad.* **11**, 505–507.